Third family quasi-Yukawa unification: Higgsino dark matter, NLSP gluino, and all that

Qaisar Shafi,[1,*] Amit Tiwari,[1,†] and Cem Salih Ün[2,3,‡]

[1]*Bartol Research Institute, Department of Physics and Astronomy, University of Delaware, Newark, Delaware 19716, USA*

[2]*Department of Physics, Bursa Uludağ University, TR16059 Bursa, Turkey*

[3]*Departamento de Ciencias Integradas y Centro de Estudios Avanzados en Física Matemáticas y Computación, Campus del Carmen, Universidad de Huelva, Huelva 21071, Spain*

(Received 26 June 2023; accepted 4 August 2023; published 18 August 2023)

We explore the implications of third family ($t-b-\tau$) quasi-Yukawa unification (QYU) for collider and dark matter (DM) searches within the framework of a supersymmetric $SU(4)_c \times SU(2)_L \times SU(2)_R$ model. The deviation from exact Yukawa unification is quantified through the relation $y_t : y_b : y_\tau = (1+C) : (1-C) : (1+3C)$, with C being a real parameter ($|C| \leq 0.2$). We allow for the breaking of left-right symmetry both by the soft scalar and gaugino mass parameters and obtain a variety of viable solutions that predict the sparticle mass spectrum including the lightest supersymmetric particle (LSP) DM (whose stability is guaranteed by a Z_2 gauge symmetry). We highlight solutions that include a next to LSP (NLSP) gluino with mass ∼1.3–2.5 TeV, which should be accessible at LHC Run 3. There also exist NSLP stop solutions with masses heavier than about 1.8 TeV, which are consistent with the LSP neutralino dark matter relic density through stop-neutralino coannihilation. We identify A-resonance solutions, which arise when the CP-odd Higgs boson is in resonance with a pair of LSP neutralinos ($m_A = 2m_{\tilde{\chi}_1^0}$) with DM mass ∼0.8–2 TeV, as well as bino-chargino, bino-slepton and bino-stau coannihilation scenarios. Finally, we also identify Wino-like (∼99%) and Higgsino-like (∼99%) solutions whose masses are heavier than about 1.5 and 1 TeV, respectively. These solutions are compatible with the desired dark matter relic density and testable in ongoing and future direct detection experiments.

DOI: 10.1103/PhysRevD.108.035027

I. INTRODUCTION

Low scale supersymmetry (SUSY) remains an attractive extension of the Standard Model (SM) for a number of reasons. First, the gauge hierarchy problem associated with quadratic divergences in the scalar sector of the SM is significantly tamed in the presence of low scale SUSY. Second, while the SM quartic Higgs coupling λ is essentially a free parameter in the SM, in the simplest supersymmetric extensions such as the minimal supersymmetric SM (MSSM), λ is related to the gauge couplings of the electroweak sector. This feature allows one to provide an estimate for the upper bound of around 130 GeV or so on the SM Higgs mass in MSSM, which is in excellent agreement with the experimentally measured value of 125.6 GeV [1,2]. Thanks to SUSY, the problem of λ running to zero and subsequently turning negative at a scale of around 10^{11} GeV is also avoided. Finally, in the presence of TeV scale SUSY, the three SM gauge couplings nicely unify at an energy scale close to 10^{16} GeV [3–6]. This last feature provides a strong motivation for considering supersymmetric grand unified theories. Other good reasons include electric charge quantization, unification of quarks and leptons in each family, and prediction of nonzero neutrino masses, which is required by the observed solar, atmospheric and reactor neutrino oscillation experiments (for a recent review and additional references see [7]). A particularly attractive example of grand unification is provided by SUSY SO(10) which, among other things, also predicts third family ($t-b-\tau$) Yukawa unification (YU) to a good approximation [8,9]. The consequences for collider and dark matter physics that follow from YU have been extensively studied in the literature (see [10] for recent discussion and additional references).

Motivated by the ongoing LHC Run 3 at CERN and the large number of dark matter searches underway, we investigate the experimental consequences of third family

*qshafi@udel.edu
†amitiit@udel.edu
‡cemsalihun@uludag.edu.tr

quasi-YU (QYU) [11–13] in the framework of $SU(4)_c \times SU(2)_L \times SU(2)_R$ (422 for short), which is a maximal subgroup of $SO(10)$ [14] and retains some of the key predictions of $SO(10)$ (for a recent discussion of b-tau Yukawa unification in 422 see Ref. [15]). We go beyond earlier investigations with the assumption that the soft SUSY breaking scalar and gaugino masses do not respect left-right symmetry, and the soft scalar masses for the first two families are split from the third family which allows us to probe a larger region of the parameter space compared to earlier studies. Such a mass splitting between the families can be realized by supplementing the GUT symmetry with a gauge group acting on the families. A detailed discussion for possible UV completions involving symmetries acting on the flavor can be found in Ref. [16] and references therein.

In this paper, we assume that the 422 symmetry broken to MSSM at $M_{\rm GUT}$. Below $M_{\rm GUT}$, the sparticle spectrum coincides with the MSSM spectrum. Note that C-parity, which interchanges left and right handed fields and also conjugates the representations, is also broken at $M_{\rm GUT}$. We have explored the predictions for sparticle masses including dark matter and NLSP candidates in the framework of a supersymmetric 422 model which incorporates third family QYU. The R–parity required in the MSSM model to prevent rapid proton decay and realize a stable LSP can be linked to the gauged Z_2 subgroup of the Z_4 center of $Spin(10)$. This Z_2 symmetry remains intact if $Spin(10)$ is broken to $SU(3)_c \times U(1)_{\rm em}$ using tensor representations [17] (for a recent discussion see, [18]). In practice, this occurs if the $B-L$ symmetry is broken using a field with $B-L$ charge of two. In general, the 422 model leads to very rich phenomenology of DM in its low scale predictions [19]. These predictions can be constrained further by considering several analyses from different experimental results. For instance, the 422 model can accommodate the muon $g-2$ solutions only for the binolike LSP neutralino, and such solutions allow several coannihilation scenarios to yield a relic abundance of LSP neutralino consistent with the current Planck measurements. Even though the QYU condition excludes muon $g-2$ solutions, we also identify winolike and Higgsinolike dark matter solutions which yield the desired DM relic abundance with masses greater than or of order 1.5 and 1 TeV, respectively. Apart from the muon $g-2$ consideration, the 422 model can maintain exact YU, which is realized for gluino NLSP lighter than about 1 TeV [20], which is close to being excluded in the current experimental analyses. In the case of QYU, on the other hand, the NLSP gluino mass lies in the 1.3–2.5 TeV, which is more likely to be tested at the LHC Run3. In addition, the mass splittings of the third and first/second families permit the stop-neutralino coannihilation scenario for stops in the 1.8–2.3 TeV mass range. Other solutions include the NLSP stau with mass between 1–2 TeV and A-resonance solutions with the mass m_A varying between 0.5 and 2.5 TeV. In this context, the A-resonance solutions can also be tested through the decay channel A, $H \longrightarrow \tau\tau$, which currently excludes the solutions with $m_A \lesssim 2$ TeV in the large $\tan\beta$ region. We should note that exact YU usually leads to a heavier mass spectrum at the low scale which excludes the stop-neutralino coannihilation scenario as well as A–resonance solutions. Even though QYU enlarges the parameter space of YU, its predictive feature comes from the solutions which are within reach of the current and near future experiments at LHC and DM detection (see, for instance, [21]).

This paper is organized as follows: In Sec. II, we briefly describe QYU, scanning procedure, the employed constraints and fundamental parameter space. In Sec. III, we display the plots for the GUT scale mass parameters and the implications for the mass spectra. Section IV is devoted to the DM implications including the relic density as well as the spin-independent and spin-dependent scattering cross sections. In this section, we display five benchmark points and discuss the prospects to test QYU in the ongoing collider and DM experiments.

II. QUASI-YUKAWA UNIFICATION, FUNDAMENTAL PARAMETERS, SCANNING PROCEDURE, AND EXPERIMENTAL CONSTRAINTS

Precise third family Yukawa unification (YU) is realized in supersymmetric unified theories based on gauge groups such as SO(10) and 422 [8,22]. Quasi-Yukawa unification (QYU) is motivated by the desire to incorporate the observed fermion masses and mixings, and a particularly simple yet realistic example of t-b-tau QYU is provided by the relation [11,23]:

$$y_t : y_b : y_\tau = (1+C) : (1-C) : (1+3C), \qquad (2.1)$$

where C is taken to be real, but it can be negative or positive. The quasi-Yukawa relation in Eq. (2.1) can be realized by including a nonzero vacuum expectations value from the (15,2,2) representation of 4-2-2 (for more details see Refs. [11,23–27]). Our main goal in this paper is to explore the phenomenological implications of this QYU condition in 422 models that can be tested in ongoing collider and dark matter experiments. Our investigation has some overlap with earlier work, but an important new ingredient here is the violation of left-right symmetry by the soft SUSY breaking parameters of the scalar and gaugino sectors of the model.

The soft supersymmetry breaking (SSB) terms in the Lagrangian include the mass terms for the scalars and gauginos, as well as trilinear interactions of the supersymmetric particles. However, these SSB terms cannot be arbitrary because of the underlying GUT symmetry. Since we consider a symmetry breaking pattern in which the LR

symmetry is also broken, the set of free parameters includes two different mass terms for the left and right handed fields. In addition, we also assume a flavor symmetry at the GUT scale that distinguishes the third family from the others, which doubles the number of mass terms for the scalar matter fields. If we assign a parameter $x_{\rm LR}$ which quantifies the LR breaking in the scalar sector, one can define the following relation for the SSB mass terms for the matter fields:

$$m_{\tilde{R}_i} = x_{\rm LR} m_{\tilde{L}_i}, \quad i = 1, 2(3) \text{ for the first two (third) families} \tag{2.2}$$

The relation among the SSB gaugino masses can be derived from the breaking of 422. When the 422 symmetry breaks to the MSSM gauge group the hypercharge generator remains unbroken and yields the following mass relation for the gauginos:

$$Y = \sqrt{\frac{3}{5}} I_{3R} + \sqrt{\frac{2}{5}}(B-L) \Rightarrow M_1 = \frac{3}{5} M_{2R} + \frac{2}{5} M_3, \tag{2.3}$$

where I_{3R} and $B-L$ are the diagonal generators of $SU(2)_R$ and $SU(4)_c$ respectively, and M_1, M_{2R}, and M_3 are the SSB mass terms for the gauginos associated with the $U(1)_Y$, $SU(2)_R$, and $SU(4)_c$ gauge groups respectively. As stated for the scalar matter fields, the LR symmetry breaking leads, in general, to $M_{2R} \neq M_{2L}$, where M_{2L} denotes the mass of the $SU(2)_L$ gaugino. If we assign a parameter $y_{\rm LR}$ to measure the LR breaking in the gaugino sector as $M_{2R} = y_{\rm LR} M_{2L}$, Eq. (2.3) yields

$$M_1 = \frac{3}{5} y_{\rm LR} M_{2L} + \frac{2}{5} M_3. \tag{2.4}$$

We can summarize the set of GUT scale free parameters and their ranges in our scans as follows:

$$\begin{aligned}
0 \leq \quad & m_{\tilde{L}_{1,2}}, m_{\tilde{L}_3} \leq 20 \text{ TeV} \\
0 \leq \quad & M_{2L} \leq 5 \text{ TeV} \\
-3 \leq \quad & M_3 \leq 5 \text{ TeV} \\
-3 \leq \quad & A_0/m_{\tilde{L}_3} \leq 3 \\
35 \leq \quad & \tan\beta \leq 60 \\
0 \leq \quad & \mathrm{x_{LR}} \leq 3 \\
-3 \leq \quad & \mathrm{y_{LR}} \leq 3 \\
0 \leq \quad & \mathrm{x_d} \leq 3 \\
-1 \leq \quad & \mathrm{x_u} \leq 2,
\end{aligned} \tag{2.5}$$

where we assume a universal trilinear coupling denoted by A_0. Note that we consider the same $x_{\rm LR}$ to quantify the LR symmetry breaking for all the families. We also impose nonuniversal Higgs boson masses at $M_{\rm GUT}$ which are parametrized as $m_{H_d} = x_d m_{\tilde{L}_3}$ and $m_{H_u} = x_u m_{\tilde{L}_3}$. Note that this parametrization is employed only to determine the magnitude of $m_{H_{d,u}}$ terms. However, in our scans, we input the square of these parameters. In this substitution, the sign of the relevant parameter (x_d for m_{H_d} and x_u for m_{H_u}) also determines the sign of the square of these parameters as $m^2_{H_{d,u}} = \mathrm{sgn}(x_{d,u})(x_{d,u} m_{H_{d,u}})^2$. This setup can determine the behavior of the solution depending especially on the sign of x_u. If $m^2_{H_u}$ is set to be positive at the GUT scale, the electroweak symmetry breaking has to be broken radiatively through the RGE equations which can be realized for $m^2_{H_u} > m^2_{H_d}$ and/or large A–terms as well as $y_t > y_b$ [28]. On the other hand, if $m^2_{H_u}$ happens to be negative at the GUT scale, such conditions may not match for a consistent electroweak symmetry breaking. Similarly, we also allow negative values for M_3. The positive values of M_3 allow one to compare the NLSP gluino solutions in QYU with exact YU, and negative M_3 values at the GUT scale yield the heavier gluino solutions.

We perform random scans in the fundamental parameter space of 422 by using SPheno [29,30] generated by SARAH [31,32] for numerical calculations. After the GUT scale is determined through renormalization group equations (RGEs) by imposing the unification condition on the SM gauge couplings as $g_1 = g_2 \simeq g_3$, the RGEs run back from $M_{\rm GUT}$ to M_Z scale together with the SSB terms determined by the parameters given in Eq. (2.5). The SUSY mass spectra are calculated at the two-loop level. In order to improve the precision in the theoretical calculations of the SM-like Higgs boson mass, we use the method which runs the SM RGEs at the three-loop level between M_Z and $M_{\rm SUSY}$ by using the effective Higgs potential and imposing the matching condition at this scale. Even though this method does not affect the uncertainties arising from the top-quark mass, the QCD coupling and the mixing in the stop sector [33], it improves the uncertainties from the logarithmic terms which might be canceled by employing higher order RGEs. Note that we insert the central value of the top quark mass ($m_t = 173.3$ GeV [34,35]). Even though $1-2\sigma$ variation in the top quark mass does not affect the SUSY spectrum, it can yield a 1–2 GeV shift in the SM-like Higgs boson mass [36,37]. In our scans, we accept only the solutions in which the LSP is one of the MSSM neutralinos. At the final step of the scans, we transfer the SPheno outputs to micrOMEGAs [38] to calculate the dark matter (DM) observables.

In the scanning procedure, we employ the Metropolis-Hastings algorithm [39,40]. After generating the data, we successively employ the mass bounds [41], constraints from combined results for rare B–meson decays [42–44], and the latest Planck Satellite measurements [45] of the DM relic abundance to constrain the LSP neutralino. We can

summarize the experimental constraints employed in our analyses as follows:

$$\begin{aligned} m_h &= 123\text{–}127 \text{ GeV} \\ m_{\tilde{g}} &\geq 2.1 \text{ TeV (800 GeV if it is NLSP)} \\ 1.95 \times 10^{-9} &\leq \text{BR}(B_s \to \mu^+\mu^-) \leq 3.43 \times 10^{-9}(2\sigma) \\ 2.99 \times 10^{-4} &\leq \text{BR}(B \to X_s\gamma) \leq 3.87 \times 10^{-4}(2\sigma) \\ 0.114 &\leq \Omega_{\text{CDM}}h^2 \leq 0.126(5\sigma). \end{aligned} \tag{2.6}$$

We have listed only the Higgs boson and gluino mass bounds, since they have been updated model independently, although we also employ the model independent mass bounds from the Linear electron-positron collider (LEP2) [46]. Even though the parameters listed in Eq. (2.6) have been measured experimentally with significant precision, we consider a few σ variations to compensate for the uncertainties in their theoretical calculations arising from strong interaction coupling, the top quark mass, the mixing in the squark sectors, etc. [33,36,47–52]. We employ a 5σ uncertainty in constraining the relic abundance of LSP neutralino since the uncertainties in its theoretical calculations exceed the statistical uncertainties in its experimental measurements [53,54].

We identify the solutions compatible with the QYU condition if the deviation in Yukawa couplings quantified by the C parameter satisfies $|C| \leq 0.2$. Bounding the deviation from exact YU as $|C| \leq 0.2$ is based on some earlier studies [23,55,56]. In more restricted models such as CMSSM, the correct fermion masses for the third family yield a range for the deviation as $0.1 \lesssim |C| \lesssim 0.25$ [11,56]. On the other hand, one can realize QYU solutions consistent with the fermion masses in a relatively larger range in more flexible models such as 422. In this context, imposing the QYU condition as $|C| \leq 0.2$ will also keep the QYU scenarios applicable in the restricted models as well. In addition, the deviation from YU bounded with C still allows us to compare QYU implications with those for exact YU in terms of the testable observables and threshold corrections, etc. Note that Eq. (2.1) leads to three different solutions for C in terms of different combinations of the Yukawa couplings. We also require the QYU compatible solutions to yield the same $|C|$ in all three Yukawa couplings up to about 10% uncertainty.

III. QYU AND MASS SPECTRUM

In this section, we display the plots for the GUT scale mass parameters in Fig. 1 with plots in the C-$m_{\tilde{L}_3}$, C-$m_{\tilde{L}_{1,2}}$, C-M_{2L} and C-M_3 planes. The fundamental parameters in the horizontal axes represent their GUT scale values imposed in our scans. All solutions are compatible with radiative electroweak symmetry breaking (REWSB) and LSP neutralino conditions. The solutions in the fade brown regions are excluded by at least one of the constraints from the mass bounds or rare B–decays, while the green points are consistent with them. Orange points form a subset of green and they represent the solutions which yield a deviation from YU in terms of C compatible with Eq. (2.1). The QYU bound on $|C|$ is shown with the horizontal dashed line, below which the orange points satisfy the QYU condition. Red points are a subset of orange and satisfy the constraint on relic abundance of LSP neutralino from Planck measurements within 5σ. Yellow points form a subset of orange with DM relic density lower than the 5σ constraints from the Planck measurements. The C-$m_{\tilde{L}_3}$ plane shows that the QYU condition on the Yukawa couplings at M_{GUT} can be realized in a wide range as $0.3 \lesssim m_{\tilde{L}_3} \lesssim 20$ TeV. The solutions with low $m_{\tilde{L}_3}$ yield a relatively large deviation from YU ($|C| \gtrsim 0.12$), and the DM relic density bounds it at about 0.18 from below (red solutions). Besides, the lighter solutions lead to the SM-like Higgs boson mass at about 123 GeV, and the central value of the Higgs boson mass (∼125.6 GeV) favors the solutions with $m_{\tilde{L}_3} \gtrsim 1$ TeV. The SSB mass term for the first two families compatible with the QYU condition can also be light, but the solutions consistent with the DM relic density can be realized if $m_{\tilde{L}_{1,2}} \gtrsim 3$ TeV, as shown in the $|C|$-$m_{\tilde{L}_{1,2}}$ plane. The bottom panels of Fig. 1. Similar observation can be seen from the bottom panels where the SSB masses for $SU(2)_L$ and $SU(3)_c$ gauginos are plotted. Note that the fade region in the C-M_3 plane ($-600 \lesssim M_3 \lesssim 600$ GeV) is excluded by the current mass bound on gluino.

The masses for the right-handed partners of the SUSY scalars and gauginos can be considered through the LR symmetry breaking parametrized by x_{LR} and y_{LR} which are displayed in Fig. 2 with plots in the C-x_{LR} and C-y_{LR} planes. Color coding is the same as in Fig. 1. The C-x_{LR} plane shows that LR breaking in the scalar sector compatible with the QYU condition and the other constraints can be measured in the range $0.7 \lesssim x_{\text{LR}} \lesssim 2.2$. Even though it is possible to realize QYU if the scalar sector is LR symmetric ($x_{\text{LR}} = 1$), as seen from the C-y_{LR} plane, QYU is mostly realized if LR symmetry is broken in the gaugino sector ($|y_{\text{LR}}| \gtrsim 1$). In addition, large LR breaking in the gaugino sector can allow very small deviations in YU ($|C| \gtrsim 2\%$). Note that such solutions are realized also for $y_{\text{LR}} \sim -1$ and $|C| \sim (1 - 1.2) \times 10^{-2}$, which can be considered recovering YU. However, these solutions yield a large relic abundance of LSP neutralino and are excluded by the current Planck measurements within 5σ.

We continue our discussion with the correlation of QYU with $\tan\beta$ and the SSB trilinear scalar interacting term in Fig. 3, which also shows the RGE evolution of the Yukawa couplings between M_{GUT} and M_Z. Color coding in the top planes is the same as in Fig. 1. The curves and vertical lines in the bottom planes are defined in the legend. The C-$\tan\beta$ plane shows a nearly linear correlation between C and

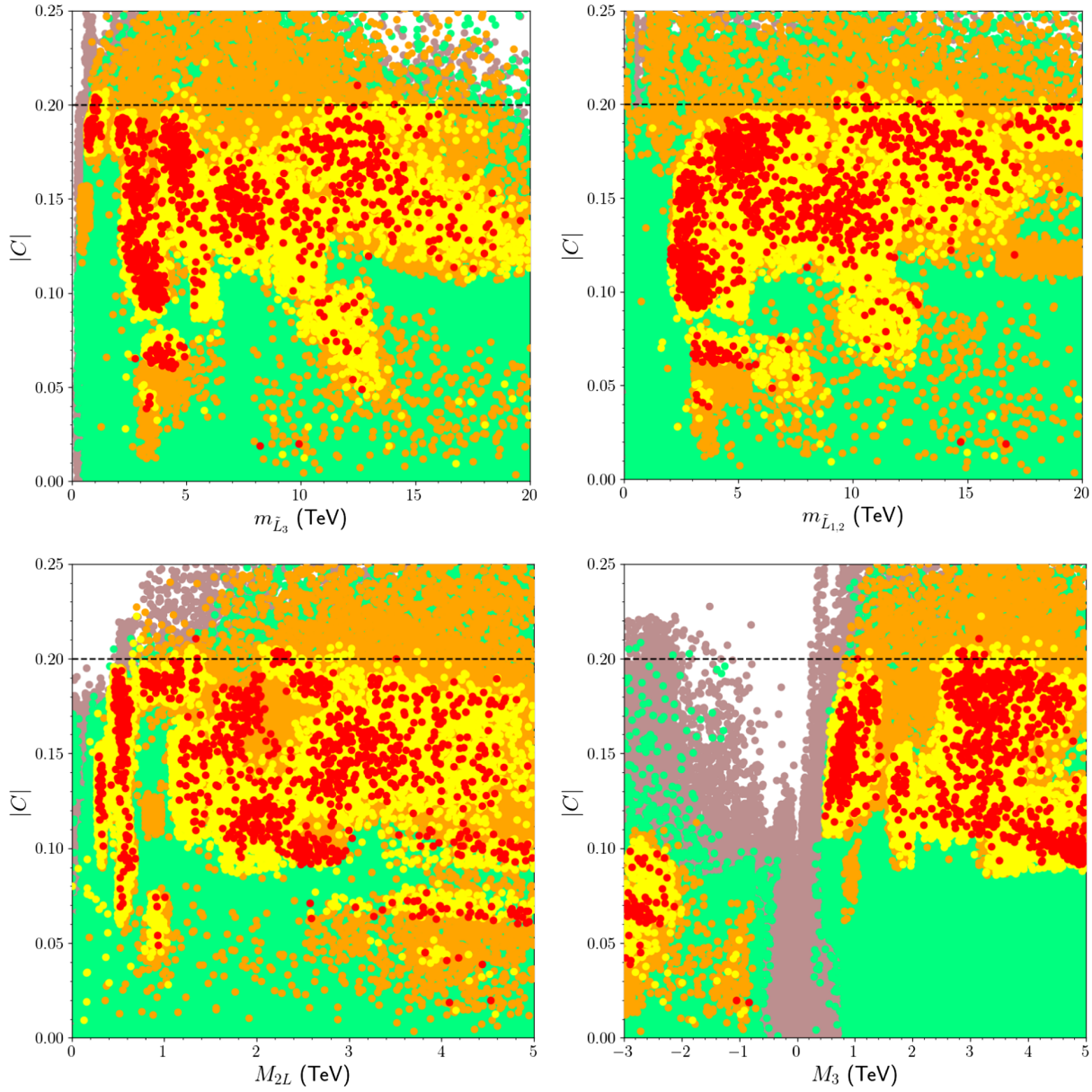

FIG. 1. Plots in the C-$m_{\tilde{L}_3}$, C-$m_{\tilde{L}_{1,2}}$, C-M_{2L}, and C-M_3 planes. All solutions are compatible with REWSB and LSP neutralino conditions. The solutions in the fade brown regions are excluded by at least one of the constraints from the mass bounds or rare B–decays, while the green points are consistent with them. Orange points form a subset of green and they represent the solutions which yield a deviation from YU in terms of C compatible with Eq. (2.1). The QYU bound on $|C|$ is shown with the horizontal dashed line, below which the orange points satisfy the QYU condition. Red points are a subset of orange and satisfy the constraint on relic abundance of LSP neutralino from Planck measurements within 5σ. Yellow points form a subset of orange with DM relic density lower than the 5σ constraints from the Planck measurements.

$\tan\beta$, which indicates that the deviation from YU increases proportionally with $\tan\beta$. One can realize a negligible deviation for $\tan\beta \sim 45$. This value of $\tan\beta$ is also suitable for exact YU (see, for instance, [10,57–59]). The results in the C-$A_0/m_{3\tilde{L}}$ plane do not show a specific correlation between C and the trilinear scalar interacting term, and the QYU condition requires $-2 \lesssim A_0/m_{3\tilde{L}} \lesssim 3$.

These relations, especially one involving $\tan\beta$, can be understood through the RGE evolution of the Yukawa couplings shown in the bottom plane of Fig. 3 for different $\tan\beta$ values. The Yukawa couplings receive threshold correction at $M_{\rm SUSY} \equiv \sqrt{m_{\tilde{t}_R} m_{\tilde{t}_L}}$, below which the SUSY particles are assumed to decouple, where $m_{\tilde{t}_{L,R}}$ stand for the left-handed and right-handed stops. These threshold corrections play an important role in realizing YU is consistent with the observed third-family fermion masses. The bottom-quark Yukawa coupling, in particular, needs large and negative threshold corrections in the case of YU [60],

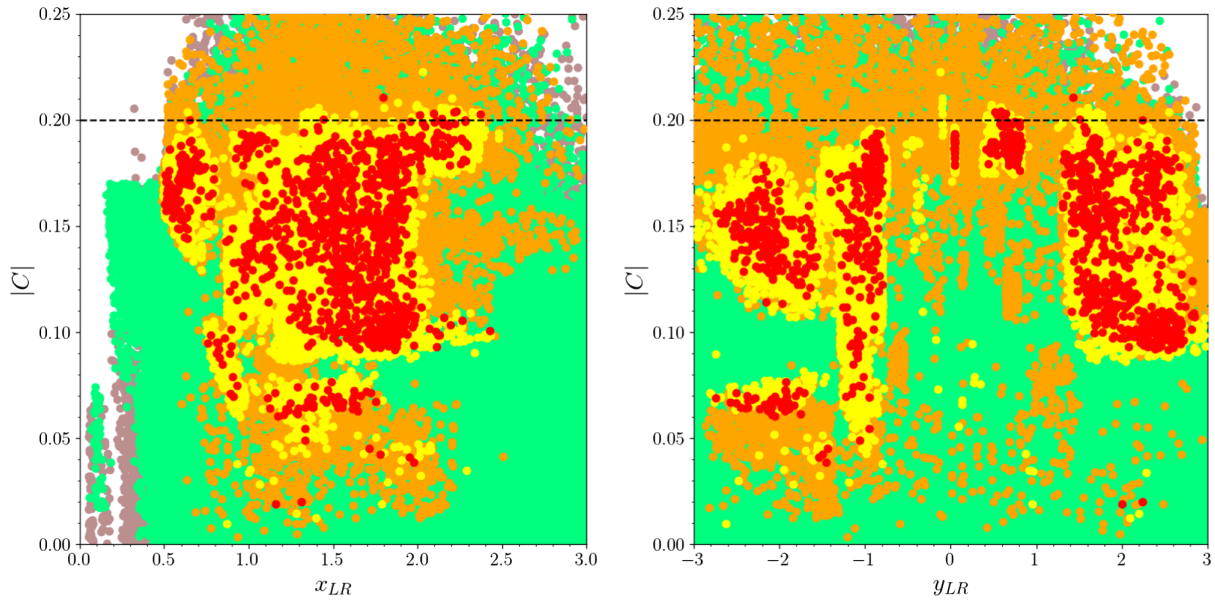

FIG. 2. Plots in the C-$x_{\rm LR}$ and C-$y_{\rm LR}$ planes. Color coding is the same as in Fig. 1.

which can be recovered in our model for $\tan\beta \sim 45$ and $|C| \sim 0$. These cases are represented with the point whose RGE evolution is shown in the bottom-left plane of Fig. 3. We note that y_b needs a negative threshold correction as large as $|\delta y_b| \simeq 0.2$ to yield a consistent bottom quark mass at M_Z. However, moving away from the YU region, the impact of the threshold corrections can be loosened. The bottom-right panel exemplifies such solutions with correct fermion masses realized even with $|\delta y_b| \sim 0.1$. Note that the curves shown crossing in the bottom figures do not indicate unification at low scales, but occur only numerically in their RGE evolution.

The impact of the threshold corrections on the parameters and mass spectrum can be seen from the following equation;

$$\delta y_b \approx \frac{g_3^2}{12\pi^2}\frac{\mu m_{\tilde{g}}\tan\beta}{m_{\tilde{b}}^2} + \frac{y_t^2}{32\pi^2}\frac{\mu A_t \tan\beta}{m_{\tilde{t}}^2}. \qquad (3.1)$$

For $\mu > 0$, the contributions from the gluino loop should be suppressed which leads to next to LSP (NLSP) gluino solutions of mass $m_{\tilde{g}} \lesssim 1$ TeV [19,20,61]. It also explains why one needs an appreciable LR breaking ($y_{\rm LR} \sim -1$, and $y_{\rm LR} \sim 2$) as shown in Fig. 2 to realize small deviations in YU ($|C| \sim 0$). However, as discussed above, the QYU solutions do not necessarily employ large threshold corrections, so the upper bound on the gluino mass from the YU condition disappears in our analyses. We display the results for the stop and gluino masses versus the LSP neutralino mass in Fig. 4 in the $m_{\tilde{t}_1}$-$m_{\tilde{\chi}_1^0}$ and $m_{\tilde{g}}$-$m_{\tilde{\chi}_1^0}$ planes. Color coding is the same as in Fig. 1. The diagonal lines designate the solutions with degenerate masses. We obtain mass spectra in which the stop mass cannot be lighter than about 1.5 TeV in the QYU parameter space (orange points), while the relic density constraint raises this lower mass bound to about 1.8 TeV (red points), where it also happens to be degenerate with the LSP neutralino in mass. These nearly degenerate solutions play an important role in reducing the relic abundance of LSP neutralino through stop-neutralino coannihilation scenario. The heavy mass scales for the stop are mostly required in order to obtain the correct SM Higgs boson mass [62]. On the other hand, we realize NLSP gluino solutions compatible with QYU condition with $m_{\tilde{g}} \gtrsim 800$ GeV, and the DM relic density constraint can be satisfied for $m_{\tilde{g}} \gtrsim 1$ TeV. The possibility of small threshold corrections also allows heavy gluino masses, and our scans yield gluino masses up to about 10 TeV. Although testing such heavy gluino solutions requires a much higher center of mass energies and luminosities than currently available at the LHC, the solutions with $2.1 \leq m_{\tilde{g}} \lesssim 2.5$ TeV should be testable during the LHC-Run3 experiments [63]. Even though we displayed the LSP masses in the plots of Fig. 4 up to 3 TeV, it can reach up to about 4 TeV. Our choice in showing the LSP mass range is mostly determined by the reach of the current and near future direct detection experiments, which will be discussed in detail in Sec. IV.

Even though we identified the green solutions as ones which are compatible with the current LHC analyses, we refer to the model-independent analyses such as those on the Higgs boson, gluino and LEP2 analyses [41]. On the other hand, these regions can be constrained further by considering the colored solutions in more detail. For instance, the strongest mass bound on the stop arises from the analyses of its decay modes involving the top quark (as in $\tilde{t} \to t\tilde{\chi}_1^0$) or b-quark (and W–boson) together with chargino. The current analyses exclude the solutions with

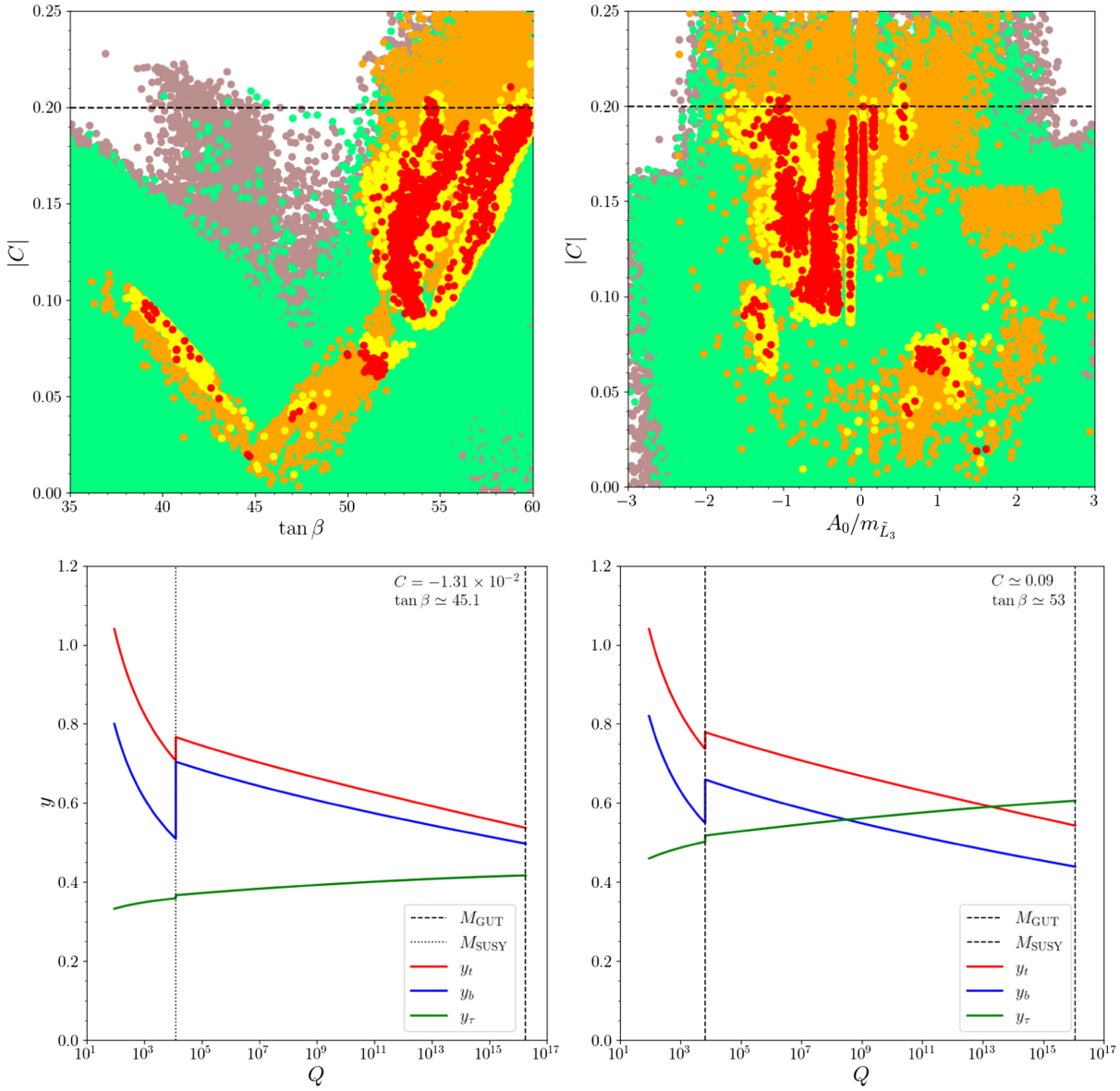

FIG. 3. Plots in the C-$A_0/m_{3\tilde{L}}$ and C- $\tan\beta$ planes (top), and the RGE evolution of the Yukawa couplings (bottom). Color coding in the top planes is the same as in Fig. 1. The curves and vertical lines in the bottom planes are defined in the panels.

$m_{\tilde{t}} \lesssim 1.2$ TeV if the LSP neutralino mass is less than about 500 GeV [64]. These results are almost model-independent if the LSP neutralino is binolike, while the lightest chargino state is formed by the wino. On the other hand, the bounds are loosened if the Higgsinos significantly mix with the MSSM gauginos in the composition of the LSP neutralino and/or chargino. Consequently these bounds do not yield a strong impact if the LSP neutralino is mostly Higgsino. If we consider the relevant region in the $m_{\tilde{t}_1}$-$m_{\tilde{\chi}_1^0}$ plane of Fig. 4, despite a strong negative impact from the SM Higgs boson mass constraint in this region mentioned above, one can accommodate a consistent Higgs boson mass in the spectrum if the mixing between the stop quarks are maximal (i.e. $X_t \simeq 2M_{\rm SUSY}$, where $X_t = A_t - \mu\cot\beta$ and $M_{\rm SUSY} = \sqrt{m_{\tilde{t}_L} m_{\tilde{t}_R}}$) [65]. However, the QYU solutions (orange) can be observed in the region where $m_{\tilde{t}_1} \gtrsim 2$ TeV and the LSP neutralino weighs less than about 500 GeV. The Planck measurements on the relic abundance of LSP neutralino (red solutions) raises this bound further up to about 5 TeV in the same region.

IV. DM IMPLICATIONS OF QYU

In general, the 422 model leads to a very rich DM phenomenology at low scales and one can identify almost all types of coannihilation scenarios, and the LSP neutralino composition which can be distinguished by identifying solutions in different regions of the

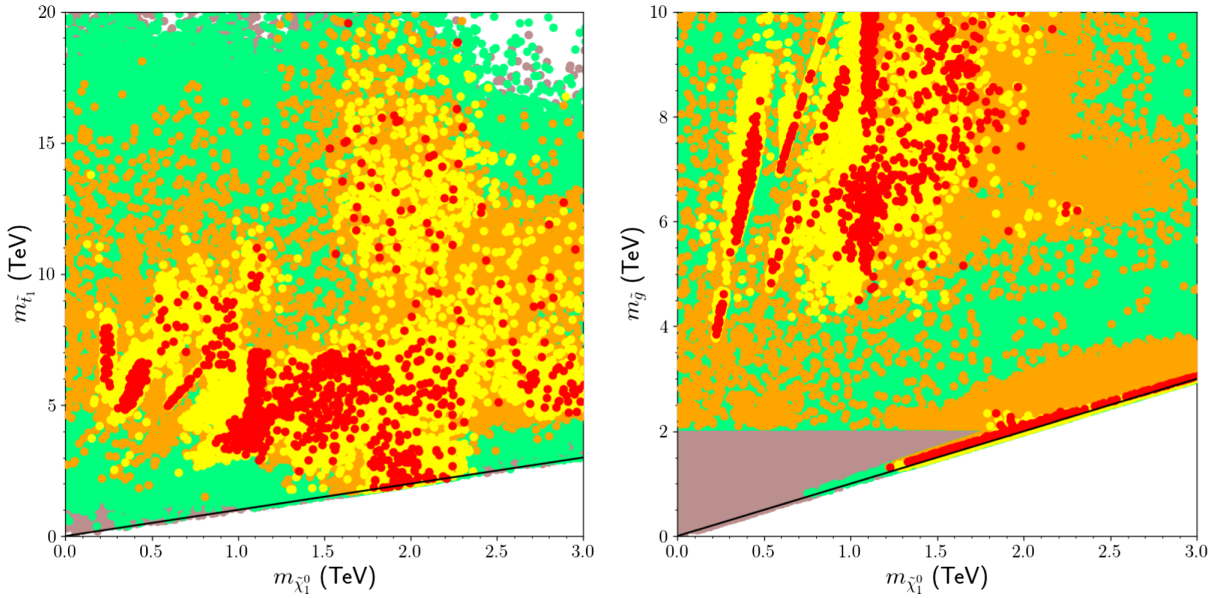

FIG. 4. Plots in the $m_{\tilde{t}_1}$-$m_{\tilde{\chi}_1^0}$ and $m_{\tilde{g}}$-$m_{\tilde{\chi}_1^0}$ planes. All solutions are compatible with REWSB and LSP neutralino conditions. Green points satisfy the mass bounds on the sparticles and the constraints from rare B-decays. Orange points form a subset of green and satisfy $|C| \leq 0.2$ as well as the QYU condition. Points in red form a subset of orange and satisfy the constraint on relic abundance of LSP neutralino from Planck measurements within 5σ. Points in yellow form a subset of orange with lower relic density than the Planck measurements. The diagonal lines represent solutions in which the particles shown are degenerate in mass.

spin-independent scattering cross section–LSP mass plane (see, for instance, [19]). On the other hand, these solutions can be further constrained by imposing the QYU condition at the GUT scale. Even though the various scenarios can remain viable after imposing the QYU condition, the latter can still exclude certain features such as the muon $g-2$ solutions [62]. In addition, although it does not seem as predictive as exact YU, it extends the variety of predictions which can be tested in the current and planned experiments. For instance, exact YU in the 422 model severely bounds the gluino mass from above at about 1 TeV, while it is possible to realize a gluino mass as heavy as about 10 TeV compatible with QYU. Such solutions are more likely to be the focus of Run3 experiments as mentioned in the previous section. In this section, we will present and discuss possible tests/probes of the QYU compatible solutions in the DM experiments by considering possible coannihilation scenarios with different species of LSP neutralino and their corresponding scattering cross sections which can be tested in the direct detection experiments.

Even though the MSSM provides a variety of different neutralino species (bino, wino, Higgsinos) as DM candidates, the current relic density and direct detection experiments have yielded a strong impact on the DM implications. The Higgsino-like LSPs usually lead to large cross sections in scattering with nuclei, and together with the relic density constraints the current results exclude the Higgsino-like LSP solutions if they are lighter than about 1 TeV (see, for instance, [66,67]). Even though their scattering cross section is moderate, the winolike LSP solutions are similarly constrained by the experiments. On the other hand, binolike LSP has a relatively small scattering cross section. However, considering the current and future projected sensitivities in the direct detection experiments [68–74], these cross sections are expected to be tested soon.

The desired DM relic density with binolike LSP requires suitable coannihilation processes, and as shown in Sec. III, this is satisfied for a gluino NLSP mass $m_{\tilde{g}} \gtrsim 1.3$ TeV. In addition, the stop-neutralino coannihilation scenario is realized for $1.8 \lesssim m_{\tilde{t}_1} \simeq m_{\tilde{\chi}_1^0} \lesssim 2.5$ TeV.

In addition, we also identify chargino-neutralino and stau-neutralino coannihilations scenarios, as well as A–resonance solutions as shown in Fig. 5, with plots in the $m_{\tilde{\chi}_1^\pm} - m_{\tilde{\chi}_1^0}$, $m_{\tilde{\tau}_1}$-$m_{\tilde{\chi}_1^0}$, m_A-$m_{\tilde{\chi}_1^0}$, and $\tan\beta$-m_A planes. The color coding is the same as in Fig. 1. The diagonal lines in the top panels indicate the mass degenerate solutions for the particles shown, and the m_A-$m_{\tilde{\chi}_1^0}$ plane displays A–resonance solutions ($m_A = 2m_{\tilde{\chi}_1^0}$). The curves in the $\tan\beta$-m_A plane display the current exclusion limits [75,76] on the CP-odd Higgs boson mass versus $\tan\beta$. The $m_{\tilde{\chi}_1^\pm}$-$m_{\tilde{\chi}_1^0}$ plane shows viable chargino-neutralino coannihilation solutions compatible with the DM abundance in a wide range with the chargino mass varying from about 250 GeV to 2.5 TeV. The solutions with $m_{\tilde{\chi}_1^0} \lesssim 1.5$ TeV around the diagonal line with the correct relic density (red points) usually lead to binolike relic density with $M_{\tilde{B}} \lesssim M_{\tilde{W}}$, since the winolike and Higgsino-like LSP solutions ($M_{\tilde{W}} \ll M_{\tilde{B}}$) are mostly excluded by the

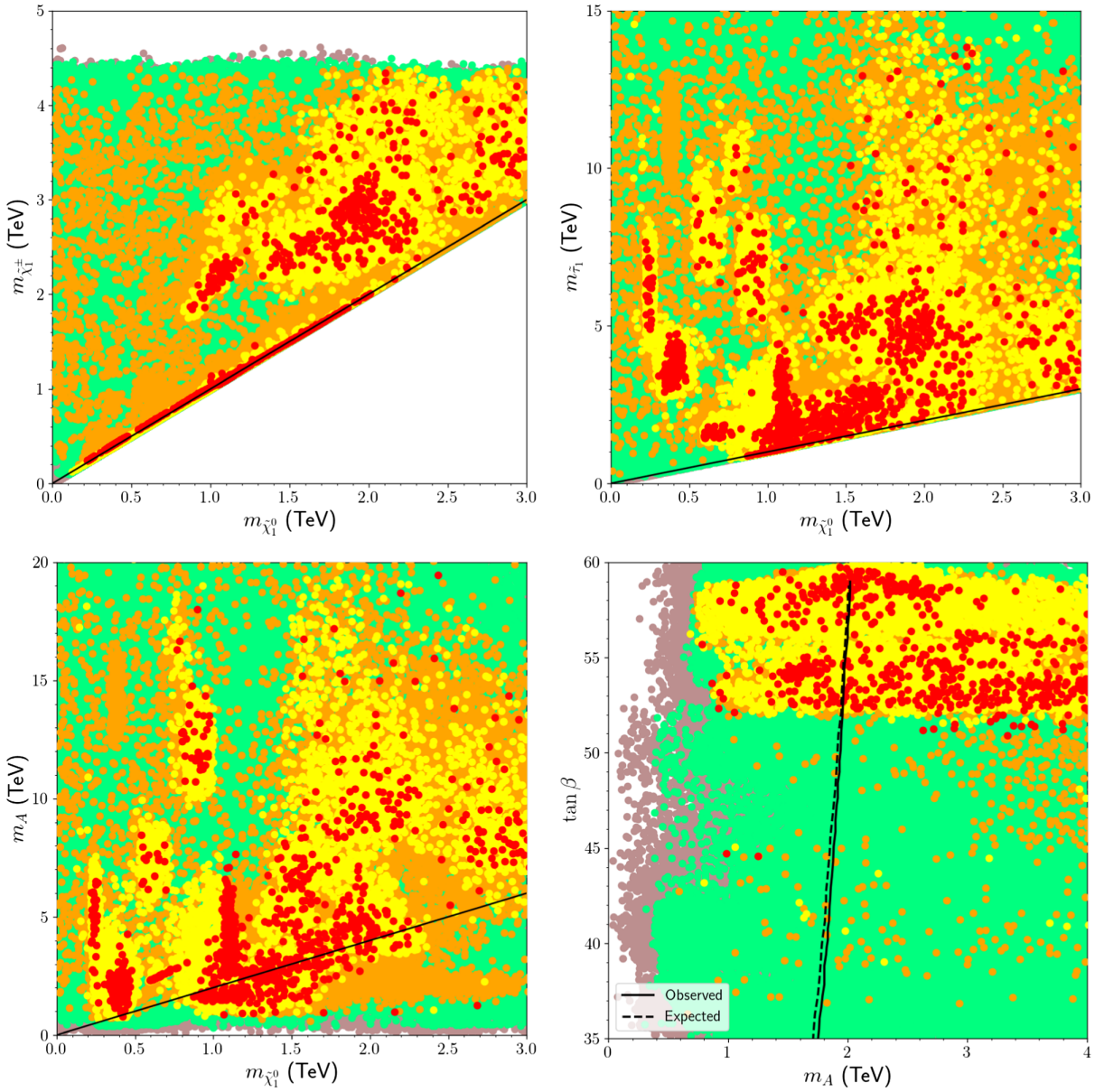

FIG. 5. Plots in the $m_{\tilde{\chi}_1^\pm}$-$m_{\tilde{\chi}_1^0}$, $m_{\tilde{\tau}_1}$-$m_{\tilde{\chi}_1^0}$, m_A-$m_{\tilde{\chi}_1^0}$, and $\tan\beta$-m_A planes. The color coding is the same as in Fig. 4. The diagonal lines in the top panels indicate the mass degenerate solutions for the particles shown, and the line in the m_A-$m_{\tilde{\chi}_1^0}$ plane represents A–resonance solutions ($m_A = 2m_{\tilde{\chi}_1^0}$). The curves in the $\tan\beta$-m_A plane display the current exclusion region [75,76] for the CP-odd Higgs boson mass.

relic density constraints for $m_{\tilde{\chi}_1^0} \lesssim 1.5$ TeV (see, for instance, [77]). We also display solutions with stau-neutralino coannihilations in the $m_{\tilde{\tau}_1}$-$m_{\tilde{\chi}_1^0}$ plane. Even though the stau is heavy over most of the parameter space due to the QYU condition, the stau-neutralino coannihilation solutions can be realized if the stau and LSP neutralino are nearly degenerate in the mass range of about 1–2.5 TeV.

As we discussed in the case of stop masses realized in our analyses, the LHC analyses [78–81] can have some impact on the MSSM gauginos and sleptons, especially in regions which can also probe the QYU solutions. However, we observed this impact on the QYU solutions with large relic density (orange), whose spectra involve binolike LSP neutralino and match the assumptions behind these analyses (i.e. bino LSP and wino chargino). Even though these solutions are available in nonstandard DM scenarios, they are excluded in our work due to the large LSP relic abundance, since we assume in our analyses that the DM relic density is saturated only by one of the MSSM neutralinos. The solutions with consistent (red) or acceptable (yellow) in the DM analyses lead to compressed spectra for $m_{\tilde{\chi}_1^\pm} - m_{\tilde{\chi}_1^0} \lesssim 3$ GeV, and a noncompressed

spectra can be realized for $m_{\tilde{\chi}_1^\pm} \gtrsim 2$ TeV. A thorough analyses performed by specialized packages [82–85] can further probe the impact on our solutions.

Besides the coannihilation channels, the QYU scenario admits self-annihilations of LSP neutralinos into the CP-odd Higgs boson in a wide range, namely $0.5 \lesssim m_A \lesssim 2.5$ TeV, as shown in the m_A-$m_{\tilde{\chi}_1^0}$ plane. The mass scale for m_A is constrained by the $A \to \tau\tau$ decay, which is displayed with the dotted and solid curves in the $\tan\beta$-m_A plane. With a mass heavier than a few hundred GeV, the neutral heavy Higgs bosons (A and H) decay into a pair of τ–leptons at a level of about 15%, which is large enough to exclude the solutions with $m_A \lesssim 2$ TeV [75,76]. A recent analysis [86] has shown that experiments at the LHC-Run3 and High-Luminosity LHC (HL-LHC) can probe the CP-odd Higgs boson up to about 2.5 TeV. Our results in the $\tan\beta$-m_A plane show that QYU solutions are abundantly realized for $2 < m_A < 2.5$ TeV, which should be tested at LHC Run-3.

Another probe for the QYU solutions can be provided in the direct detection experiments of DM. Figure 6 shows our results for the cross sections for the spin-independent (left) and spin-dependent (right) scattering of DM on nuclei versus the LSP mass. The color coding is the same as in Fig. 1. The solid (dashed) curves represent the current (future projected) exclusion curves from several direct detection DM experiments, with color coding given in the legend for each plane. The $\sigma_{\rm SI} - m_{\tilde{\chi}_1^0}$ shows that the LZ experiment [68] can currently exclude the QYU solutions with spin-independent cross section of the order of about 4×10^{-11} pb and the LSP of about 1 TeV, while XENON1T has extended this exclusion limit to about 4×10^{-12} pb in the same region. The solutions whose cross sections are above these bounds will be retested by the Darwin experiment in the near future [69]. Furthermore, the projected sensitivity of XENON experiment (the curve from XENONnT) should be able to probe QYU solutions at the level of about 8×10^{-13} pb [70]. We also present our results for the spin-dependent scattering cross section, and as seen from the $\sigma_{\rm SD} - m_{\tilde{\chi}_1^0}$, with the cross sections a few orders of magnitude lower than the experimental bounds [71–74], we have to wait for further upgrades in the experiments listed in the legend. Note that the stripes at the bottom of the left panel of Fig. 6 are the artifacts from our plotting program.

Finally, before concluding, we present six benchmark points in Table I which exemplify our findings. All points are selected to be consistent with the constraints applied in our analyses together with the QYU condition. All masses are given in GeV, and the DM scattering cross sections are in pb. For each benchmark point, the LSP and NLSP masses are shown in italics, and the masses of particles that are relevant to the discussion in bold. Point 1 represents binolike LSP neutralino solutions whose spin-independent scattering cross section lies just below the current exclusion bound provided by the XENON1T experiment, and it is expected to be tested very soon. These solutions will also be tested by Darwin. Since the spectrum involves heavy SUSY scalars, the relic abundance of LSP neutralino for such solutions can be reconciled with the Planck

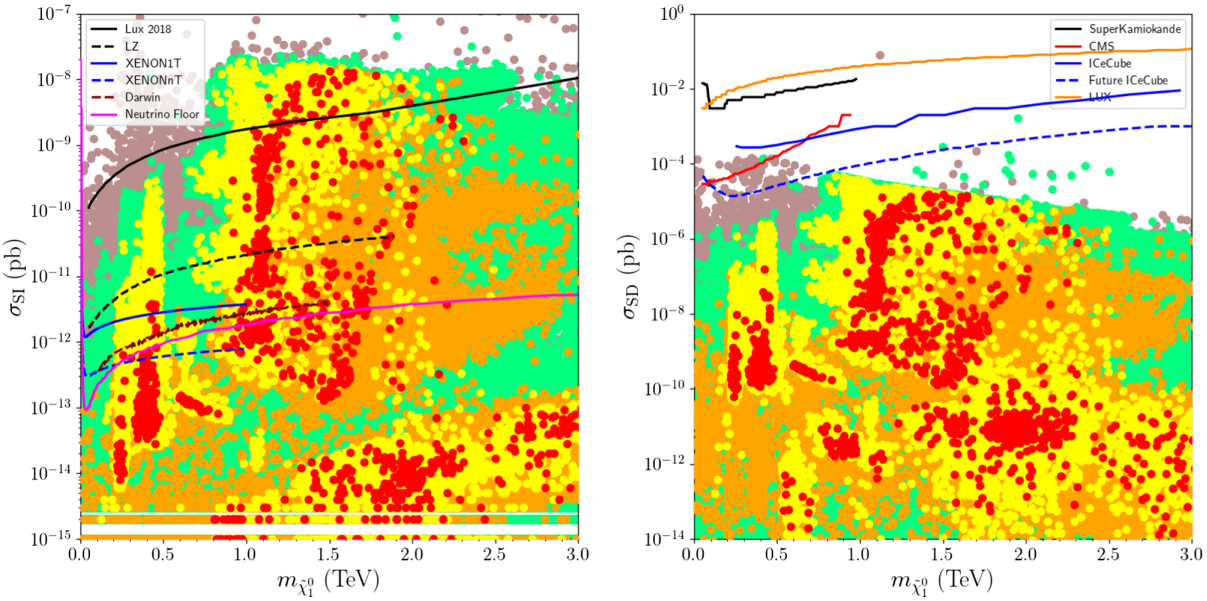

FIG. 6. Spin-independent (left) and spin-dependent (right) scattering cross sections versus the LSP neutralino mass. The color coding is the same as in Fig. 4. The curves represent the current and projected exclusion curves from several direct detection DM experiments, with the color coding given in the respective panels. The current excluded regions are represented by the solid curves, and the dashed curves display the projected experimental sensitivity.

TABLE I. Benchmark points satisfying the mass bounds, the constraints from rare B-meson decays, Planck bounds within 5σ and the QYU condition with $|C| \leq 0.2$. All masses are given in GeV. Point 1 represents chargino-neutralino coannihilation, and Point 2 exemplifies solutions in which the DM relic density is satisfied entirely through the gluino-neutralino coannihilation processes, while Point 3 depicts solutions for the stop-neutralino coannihilation scenario. Point 4 displays solutions for stau-neutralino coannihilation scenario. Points 5 and 6 represent the solutions for winolike and Higgsino-like LSP neutralino solutions respectively.

	Point 1	Point 2	Point 3	Point 4	Point 5	Point 6
$m_{\tilde{L}_{1,2}}$	5016	9007	10049	3037	5063	2981
$m_{\tilde{L}_3}$	5316	7167	8031	2493	4562	3153
M_1	998.7	−2638	−3842	2544	**3672**	7675
M_2	585.1	2803	2853	1390	**1989**	4797
M_3	3564	484.3	727.4	2990	4313	4230
$A_0/m_{\tilde{L}_3}$	−0.191	−1.5	−2	−0.793	−0.76	−1.1
$\tan\beta$	55.4	52.2	54.1	54.8	55.8	53.1
x_{LR}	1.3	1.6	1.8	1.6	1.7	2.1
y_{LR}	−1.2	−1.7	−2.4	1.6	1.6	2.1
$m_{\tilde{R}_{1,2}}$	6405	14051	18517	4782	8748	6298
$m_{\tilde{R}_3}$	6788	11181	14799	3926	7884	6662
μ	1627	8762	10877	2807	5327	**1086**
m_h	125	124	125.7	123.9	125.3	125.6
m_H	2973	4973	4660	3578	3878	2447
m_A	2973	4973	4660	3578	3878	**2447**
$m_{H^\pm}$	2974	4972	4655	3579	3877	2450
$m_{\tilde{\chi}_1^0}, m_{\tilde{\chi}_2^0}$	*426.6*, *454.7*	*1227*, 2466	*1785*, 2496	*1137*, *1153*	*1674*, *1676*	*1087*, *1090*
$m_{\tilde{\chi}_3^0}, m_{\tilde{\chi}_4^0}$	1632, 1634	8691, 8691	10915, 10915	2815, 2817	5326, 5326	3520, 3992
$m_{\tilde{\chi}_1^\pm}, m_{\tilde{\chi}_2^\pm}$	*454.8*, 1634	2466, 8691	2496, 10915	*1153*, 2817	*1677*, 5327	*1088*, 3991
$m_{\tilde{g}}$	7509	*1319*	1914	6258	8920	8621
$m_{\tilde{u}_1}, m_{\tilde{u}_2}$	7854, 8783	9098, 14023	10080, 18539	6031, 7012	8835, 11306	8184, 9612
$m_{\tilde{t}_1}, m_{\tilde{t}_2}$	6035, 7065	4052, 9017	*1873*, 11948	4534, 5196	6633, 8771	5864, 7613
$m_{\tilde{d}_1}, m_{\tilde{d}_2}$	7854, 8814	9098, 14101	10080, 18591	6031, 7041	8836, 11304	8185, 9493
$m_{\tilde{b}_1}, m_{\tilde{b}_2}$	6037, 7621	4050, 9465	1869, 12879	4539, 5596	6634, 9494	5867, 8105
$m_{\tilde{\nu}_e}, m_{\tilde{\nu}_\tau}$	3971, 4981	5419, 9107	4916, 10153	1224, 3124	3115, 5210	3009, 4428
$m_{\tilde{e}_1}, m_{\tilde{e}_2}$	4978, 6444	9100, 14155	10142, 18617	3122, 4931	5206, 8864	4424, 6894
$m_{\tilde{\tau}_1}, m_{\tilde{\tau}_2}$	3971, 4706	5419, 8903	4916, 11641	*1219*, 2497	3115, 6198	3011, 5357
σ_{SI}	2.22×10^{-12}	4×10^{-15}	2×10^{-15}	2.04×10^{-12}	3.01×10^{-12}	2.82×10^{-11}
σ_{SD}	2.78×10^{-8}	1.2×10^{-11}	5.2×10^{-12}	3.91×10^{-9}	2.68×10^{-9}	7.27×10^{-8}
Ωh^2	0.121	0.121	0.12	0.122	0.115	0.117
C	0.107	0.117	0.155	0.17	0.177	0.093

measurements through chargino-neutralino coannihilation processes. Point 2 exemplifies solutions in which the DM relic density is satisfied entirely through gluino-neutralino coannihilation processes with $m_{\tilde{g}} \gtrsim 1.3$ TeV. We exemplify the stop-neutralino coannihilation scenario with Point 3. Points 2 and 3 also represent binolike LSP solutions, but in comparison with Point 1, they lead to small spin-independent scattering cross sections which fall below the neutrino floor and need more statistics to be tested in the direct detection DM experiments. Point 4 displays a stau-neutralino coannihilation scenario, and we observe that this is accompanied by chargino-neutralino coannihilation processes in order to achieve the desired dark matter relic abundance. Even though the LSP is Bino-like as in the previous points, it should be testable in direct detection experiments in the near future. Points 5 and 6 depict solutions for winolike and Higgsino-Like LSP solutions, with masses greater than about 1.5 TeV, and 1 TeV respectively. Point 6 also depicts a spectrum in which the CP-odd Higgs boson mass is about 2.5 TeV, which should be testable at HL-LHC through $A, H \to \tau\tau$ events.

V. CONCLUSION

We have explored the predictions for sparticle masses including dark matter and NLSP candidates in the framework of a supersymmetric $SU(4)_c \times SU(2)_L \times SU(2)_R$ model which incorporates third family quasi-Yukawa unification. An unbroken Z_2 gauge symmetry contained in the 422 model acts as matter parity and ensures the presence of a viable neutralino dark matter candidate. Our solutions contain binolike, winolike, and Higgsino-like DM solutions accompanied by a variety of NLSP candidates including gluino, stop, stau and chargino. The NLSP gluino can be as light as 1.3 TeV, which should be accessible at the LHC Run 3, while stop-neutralino coannihilations become relevant for $1.8 \lesssim m_{\tilde{t}_1} \simeq m_{\tilde{\chi}_1^0} \lesssim 2.3$ TeV. The NLSP slepton masses are in the 0.9–3 TeV range, and these solutions are also involved in chargino-neutralino coannihilation processes in order to realize a consistent relic density of LSP neutralino. The winolike and Higgsino-like LSP neutralino solutions are associated with masses of order 1.5 and 1 TeV respectively. There also exist A-resonance solutions with the m_A mass varying between 0.5 and 2.5 TeV. In this context, the A-resonance solutions can also be tested through the decay channel $A, H \longrightarrow \tau\tau$, which currently excludes solutions with $m_A \lesssim 2$ TeV in the large $\tan\beta$ region. We display several benchmark points that highlight these solutions and show that the dark matter neutralino may be accessible in collider and other dark matter searches.

ACKNOWLEDGMENTS

A. T. is partially supported by the Bartol Research Institute, University of Delaware. The research of C. S. U. is supported in part by the Spanish MICINN, under Grant No. PID2019–107844GB-C22. C. S. U. would like to thank Instituto Física Theórica of Universidad Autónoma de Madrid, where part of his research has been conducted. We acknowledge Information Technologies (IT) resources at the University of Delaware, specifically the high performance computing resources for the calculation of results presented in this paper. C. S. U. also acknowledges the resources supporting this work in part were provided by the CEAFMC and Universidad de Huelva High Performance Computer (HPC@UHU) located in the Campus Universitario el Carmen and funded by FEDER/MINECO Project No. UNHU-15CE-2848.

[1] ATLAS Collaboration, Observation of a new particle in the search for the standard model Higgs boson with the ATLAS detector at the LHC, Phys. Lett. B **716**, 1 (2012).
[2] CMS Collaboration, Observation of a new boson with mass near 125 GeV in pp collisions at $\sqrt{s} = 7$ and 8 TeV, J. High Energy Phys. 06 (2013) 081.
[3] S. Dimopoulos, S. Raby, and F. Wilczek, Supersymmetry and the scale of unification, Phys. Rev. D **24**, 1681 (1981).
[4] U. Amaldi, W. de Boer, and H. Furstenau, Comparison of grand unified theories with electroweak and strong coupling constants measured at LEP, Phys. Lett. B **260**, 447 (1991).
[5] J. R. Ellis, S. Kelley, and D. V. Nanopoulos, Probing the desert using gauge coupling unification, Phys. Lett. B **260**, 131 (1991).
[6] P. Langacker and M.-x. Luo, Implications of precision electroweak experiments for M_t, ρ_0, $\sin^2\theta_W$ and grand unification, Phys. Rev. D **44**, 817 (1991).
[7] J. A. Formaggio, A. L. C. de Gouvêa, and R. G. H. Robertson, Direct measurements of neutrino mass, Phys. Rep. **914**, 1 (2021).
[8] B. Ananthanarayan, G. Lazarides, and Q. Shafi, Top mass prediction from supersymmetric guts, Phys. Rev. D **44**, 1613 (1991).
[9] B. Ananthanarayan, G. Lazarides, and Q. Shafi, Radiative electroweak breaking and sparticle spectroscopy with tan $\beta \simeq m_t/m_b$, Phys. Lett. B **300**, 245 (1993).
[10] M. E. Gómez, Q. Shafi, and C. S. Un, Testing Yukawa unification at LHC run-3 and HL-LHC, J. High Energy Phys. 07 (2020) 096.
[11] S. Dar, I. Gogoladze, Q. Shafi, and C. S. Un, Sparticle spectroscopy with neutralino dark matter from t-b-τ quasi-Yukawa unification, Phys. Rev. D **84**, 085015 (2011).
[12] Q. Shafi, S. H. Tanyıldızı, and C. S. Un, Neutralino dark matter and other LHC predictions from quasi Yukawa unification, Nucl. Phys. **B900**, 400 (2015).
[13] Z. Altın, O. Özdal, and C. S. Un, Muon $g-2$ in an alternative quasi-Yukawa unification with a less fine-tuned seesaw mechanism, Phys. Rev. D **97**, 055007 (2018).
[14] J. C. Pati and A. Salam, Lepton number as the fourth color, Phys. Rev. D **10**, 275 (1974).
[15] W. Ahmed, M. Belfkir, S. Nasri, S. Raza, and U. Zubair, LHC run-3, $b-\tau$ Yukawa unification and dark matter implications in SUSY 4-2-2 model, Phys. Rev. D **108**, 015016 (2023).
[16] K. S. Babu, I. Gogoladze, Q. Shafi, and C. S. Ün, Muon $g-2$, 125 GeV Higgs boson, and neutralino dark matter in a flavor symmetry-based MSSM, Phys. Rev. D **90**, 116002 (2014).
[17] T. W. B. Kibble, G. Lazarides, and Q. Shafi, Walls bounded by strings, Phys. Rev. D **26**, 435 (1982).
[18] G. Lazarides, Q. Shafi, and A. Tiwari, Composite topological structures in SO(10), J. High Energy Phys. 05 (2023) 119.

[19] I. Gogoladze, R. Khalid, and Q. Shafi, Yukawa unification and neutralino dark matter in $SU(4)_c \times SU(2)_L \times SU(2)_R$, Phys. Rev. D **79**, 115004 (2009).
[20] S. Raza, Q. Shafi, and C. S. Ün, NLSP gluino and NLSP stop scenarios from $b-\tau$ Yukawa unification, Phys. Rev. D **92**, 055010 (2015).
[21] A. Hebbar, Q. Shafi, and C. S. Un, Light Higgsinos, heavy gluino, and $b-\tau$ quasi-Yukawa unification: Prospects for finding the gluino at the LHC, Phys. Rev. D **95**, 115026 (2017).
[22] B. Ananthanarayan, Q. Shafi, and X. M. Wang, Improved predictions for top quark, lightest supersymmetric particle, and Higgs scalar masses, Phys. Rev. D **50**, 5980 (1994).
[23] M. E. Gomez, G. Lazarides, and C. Pallis, Yukawa quasi-unification, Nucl. Phys. **B638**, 165 (2002).
[24] B. Bajc, A. Melfo, G. Senjanovic, and F. Vissani, The minimal supersymmetric grand unified theory. 1. Symmetry breaking and the particle spectrum, Phys. Rev. D **70**, 035007 (2004).
[25] S. Bertolini, M. Frigerio, and M. Malinsky, Fermion masses in SUSY SO(10) with type II seesaw: A non-minimal predictive scenario, Phys. Rev. D **70**, 095002 (2004).
[26] B. Dutta, Y. Mimura, and R. N. Mohapatra, CKM *CP* violation in a minimal SO(10) model for neutrinos and its implications, Phys. Rev. D **69**, 115014 (2004).
[27] T. Fukuyama, A. Ilakovac, T. Kikuchi, S. Meljanac, and N. Okada, SO(10) group theory for the unified model building, J. Math. Phys. (N.Y.) **46**, 033505 (2005).
[28] S. P. Martin, A supersymmetry primer, Adv. Ser. Dir. High Energy Phys. **18**, 1 (1998).
[29] W. Porod, SPheno, a program for calculating supersymmetric spectra, SUSY particle decays and SUSY particle production at e^+e^- colliders, Comput. Phys. Commun. **153**, 275 (2003).
[30] W. Porod and F. Staub, SPheno 3.1: Extensions including flavour, *CP*-phases and models beyond the MSSM, Comput. Phys. Commun. **183**, 2458 (2012).
[31] F. Staub, SARAH, arXiv:0806.0538.
[32] F. Staub, Introduction to SARAH and related tools, Proc. Sci. CORFU2015 (**2016**) 027 [arXiv:1509.07061].
[33] G. Degrassi, S. Heinemeyer, W. Hollik, P. Slavich, and G. Weiglein, Towards high precision predictions for the MSSM Higgs sector, Eur. Phys. J. C **28**, 133 (2003).
[34] CDF and D0 Collaborations, Combination of CDF and D0 results on the mass of the top quark, arXiv:0903.2503.
[35] ATLAS Collaboration, A precise interpretation for the top quark mass parameter in ATLAS Monte Carlo simulation, Report No. ATL-PHYS-PUB-2021-034.
[36] M. Adeel Ajaib, I. Gogoladze, Q. Shafi, and C. S. Un, A predictive Yukawa unified SO(10) model: Higgs and sparticle masses, J. High Energy Phys. 07 (2013) 139.
[37] I. Gogoladze, R. Khalid, S. Raza, and Q. Shafi, Top quark and Higgs boson masses in supersymmetric models, J. High Energy Phys. 04 (2014) 109.
[38] G. Bélanger, F. Boudjema, A. Goudelis, A. Pukhov, and B. Zaldivar, micrOMEGAs5.0: Freeze-in, Comput. Phys. Commun. **231**, 173 (2018).
[39] H. Baer, S. Kraml, S. Sekmen, and H. Summy, Dark matter allowed scenarios for Yukawa-unified SO(10) SUSY GUTs, J. High Energy Phys. 03 (2008) 056.
[40] G. Belanger, F. Boudjema, A. Pukhov, and R. K. Singh, Constraining the MSSM with universal gaugino masses and implication for searches at the LHC, J. High Energy Phys. 11 (2009) 026.
[41] Particle Data Group, Review of particle physics, Chin. Phys. C **38**, 090001 (2014).
[42] CMS Collaboration, Combination of the ATLAS, CMS and LHCb results on the $B^0_{(s)} \to \mu^+\mu^-$ decays, Report No. CMS-PAS-BPH-20-003.
[43] Belle-II Collaboration, Measurement of the photon-energy spectrum in inclusive $B \to X_s\gamma$ decays identified using hadronic decays of the recoil B meson in 2019-2021 Belle II data, arXiv:2210.10220.
[44] HFLAV Collaboration, Averages of b-hadron, c-hadron, and τ-lepton properties as of 2021, Phys. Rev. D **107**, 052008 (2023).
[45] Planck Collaboration, Planck 2018 results. I. Overview and the cosmological legacy of Planck, Astron. Astrophys. **641**, A1 (2020).
[46] Particle Data Group, Review of particle physics, Chin. Phys. C **38**, 090001 (2014).
[47] I. Gogoladze, Q. Shafi, and C. S. Un, Higgs boson mass from t-b-τ Yukawa unification, J. High Energy Phys. 08 (2012) 028.
[48] H. Bahl, S. Heinemeyer, W. Hollik, and G. Weiglein, Theoretical uncertainties in the MSSM Higgs boson mass calculation, Eur. Phys. J. C **80**, 497 (2020).
[49] E. Bagnaschi, J. Pardo Vega, and P. Slavich, Improved determination of the Higgs mass in the MSSM with heavy superpartners, Eur. Phys. J. C **77**, 334 (2017).
[50] P. Athron, J.-h. Park, T. Steudtner, D. Stöckinger, and A. Voigt, Precise Higgs mass calculations in (non-)minimal supersymmetry at both high and low scales, J. High Energy Phys. 01 (2017) 079.
[51] B. C. Allanach, A. Djouadi, J. L. Kneur, W. Porod, and P. Slavich, Precise determination of the neutral Higgs boson masses in the MSSM, J. High Energy Phys. 09 (2004) 044.
[52] P. Drechsel, R. Gröber, S. Heinemeyer, M. M. Muhlleitner, H. Rzehak, and G. Weiglein, Higgs-boson masses and mixing matrices in the NMSSM: Analysis of on-shell calculations, Eur. Phys. J. C **77**, 366 (2017).
[53] P. Bergeron, P. Sandick, and K. Sinha, Theoretical uncertainties in the calculation of supersymmetric dark matter observables, J. High Energy Phys. 05 (2018) 113.
[54] H. Baer, V. Barger, and D. Martinez, Comparison of SUSY spectra generators for natural SUSY and string landscape predictions, Eur. Phys. J. C **82**, 172 (2022).
[55] M. E. Gomez, G. Lazarides, and C. Pallis, On Yukawa quasiunification with mu less than 0, Phys. Rev. D **67**, 097701 (2003).
[56] N. Karagiannakis, G. Lazarides, and C. Pallis, CMSSM with Yukawa quasi-unification revisited, Phys. Lett. B **704**, 43 (2011).
[57] M. Hussain and R. Khalid, Yukawa unification with light supersymmetric particles consistent with LHC constraints, Nucl. Phys. **B942**, 30 (2019).
[58] S. Antusch, C. Hohl, and V. Susič, Comparatively light extra Higgs states as signature of SUSY SO(10) GUTs with 3rd family Yukawa unification, J. High Energy Phys. 06 (2020) 014.

[59] Y. Hiçyılmaz, $t-b-\tau$ Yukawa unification in non-holomorphic MSSM, J. High Energy Phys. 04 (2021) 218.
[60] I. Gogoladze, R. Khalid, S. Raza, and Q. Shafi, $t-b-\tau$ Yukawa unification for $\mu<0$ with a sub-TeV sparticle spectrum, J. High Energy Phys. 12 (2010) 055.
[61] I. Gogoladze, R. Khalid, and Q. Shafi, Coannihilation scenarios and particle spectroscopy in $SU(4)_c \times SU(2)_L \times SU(2)_R$, Phys. Rev. D **80**, 095016 (2009).
[62] M. E. Gomez, Q. Shafi, A. Tiwari, and C. S. Un, Muon $g-2$, neutralino dark matter and stau NLSP, Eur. Phys. J. C **82**, 561 (2022).
[63] ATLAS Collaboration, SUSY summary plots March 2022, Report No. ATL-PHYS-PUB-2022-013.
[64] CMS Collaboration, Search for direct top squark pair production in events with one lepton, jets, and missing transverse momentum at 13 TeV with the CMS experiment, J. High Energy Phys. 05 (2020) 032.
[65] F. Brummer, S. Kraml, and S. Kulkarni, Anatomy of maximal stop mixing in the MSSM, J. High Energy Phys. 08 (2012) 089.
[66] S. Raza, Q. Shafi, and C. S. Un, $b-\tau$ Yukawa unification in SUSY SU(5) with mirage mediation: LHC and dark matter implications, J. High Energy Phys. 05 (2019) 046.
[67] Y. Hiçyılmaz, L. Selbuz, L. Solmaz, and C. S. Ün, Model characterization and dark matter in the secluded U(1)' model, Phys. Rev. D **105**, 055029 (2022).
[68] LZ Collaboration, Projected WIMP sensitivity of the LUX-ZEPLIN dark matter experiment, Phys. Rev. D **101**, 052002 (2020).
[69] DARWIN Collaboration, DARWIN: Towards the ultimate dark matter detector, J. Cosmol. Astropart. Phys. 11 (2016) 017.
[70] XENON Collaboration, Projected WIMP sensitivity of the XENONnT dark matter experiment, J. Cosmol. Astropart. Phys. 11 (2020) 031.
[71] Super-Kamiokande Collaboration, An indirect search for WIMPs in the sun using 3109.6 days of upward-going muons in Super-Kamiokande, Astrophys. J. **742**, 78 (2011).
[72] CMS Collaboration, Search for dark matter, extra dimensions, and unparticles in monojet events in proton–proton collisions at $\sqrt{s}=8$ TeV, Eur. Phys. J. C **75**, 235 (2015).
[73] IceCube Collaboration, Limits on a Muon Flux from Neutralino Annihilations in the Sun with the IceCube 22-String Detector, Phys. Rev. Lett. **102**, 201302 (2009).
[74] LUX Collaboration, Results on the Spin-Dependent Scattering of Weakly Interacting Massive Particles on Nucleons from the Run 3 Data of the LUX Experiment, Phys. Rev. Lett. **116**, 161302 (2016).
[75] E. Bagnaschi *et al.*, MSSM Higgs boson searches at the LHC: Benchmark scenarios for run 2 and beyond, Eur. Phys. J. C **79**, 617 (2019).
[76] ATLAS Collaboration, Search for Heavy Higgs Bosons Decaying into Two Tau Leptons with the ATLAS Detector Using pp Collisions at $\sqrt{s}=13$ TeV, Phys. Rev. Lett. **125**, 051801 (2020).
[77] M. Frank, Y. Hiçyılmaz, S. Mondal, O. Özdal, and C. S. Ün, Electron and muon magnetic moments and implications for dark matter and model characterisation in non-universal U(1)' supersymmetric models, J. High Energy Phys. 10 (2021) 063.
[78] ATLAS Collaboration, Search for charginos and neutralinos in final states with two boosted hadronically decaying bosons and missing transverse momentum in pp collisions at $\sqrt{s}=13$ TeV with the ATLAS detector, Report No. ATLAS-CONF-2021-022.
[79] ATLAS Collaboration, Search for direct production of electroweakinos in final states with one lepton, missing transverse momentum and a Higgs boson decaying into two b-jets in pp collisions at $\sqrt{s}=13$ TeV with the ATLAS detector, Eur. Phys. J. C **80**, 691 (2020).
[80] ATLAS Collaboration, Search for chargino and neutralino production in final states with a Higgs boson and missing transverse momentum at $\sqrt{s}=13$ TeV with the ATLAS detector, Phys. Rev. D **100**, 012006 (2019).
[81] ATLAS Collaboration, Search for electroweak production of supersymmetric particles in final states with two or three leptons at $\sqrt{s}=13$ TeV with the ATLAS detector, Eur. Phys. J. C **78**, 995 (2018).
[82] CheckMATE Collaboration, Constraining electroweak and strongly charged long-lived particles with CheckMATE, Eur. Phys. J. C **81**, 968 (2021).
[83] G. Alguero, J. Heisig, C. K. Khosa, S. Kraml, S. Kulkarni, A. Lessa *et al.*, Constraining new physics with SModelS version 2, J. High Energy Phys. 08 (2022) 068.
[84] J. Alwall, M. Herquet, F. Maltoni, O. Mattelaer, and T. Stelzer, MadGraph 5: Going beyond, J. High Energy Phys. 06 (2011) 128.
[85] A. Belyaev, N. D. Christensen, and A. Pukhov, CalcHEP 3.4 for collider physics within and beyond the standard model, Comput. Phys. Commun. **184**, 1729 (2013).
[86] CMS Collaboration, Projection of the Run 2 MSSM $H \to \tau\tau$ limits for the high-luminosity LHC, Report No. CMS-PAS-FTR-18-017.